Physics and Imaging in Radiation Oncology 31 (2024) 100603

Contents lists available at ScienceDirect

Physics and Imaging in Radiation Oncology

journal homepage: www.sciencedirect.com/journal/physics-and-imaging-in-radiation-oncology

Original Research Article

Multi-modality imaging parameters that predict rapid tumor regression in head and neck radiotherapy

Eric Aliotta [a,*], Ramesh Paudyal [a], Bill Diplas [b], James Han [b], Yu-Chi Hu [a], Jung Hun Oh [a], Vaios Hatzoglou [c], Naomi Jensen [a], Peng Zhang [a], Michalis Aristophanous [a], Nadeem Riaz [b], Joseph O. Deasy [a], Nancy Y. Lee [b,1], Amita Shukla-Dave [a,c,1]

[a] Department of Medical Physics, Memorial Sloan Kettering Cancer Center, New York, NY
[b] Department of Radiation Oncology, Memorial Sloan Kettering Cancer Center, New York, NY
[c] Department of Radiology, Memorial Sloan Kettering Cancer Center, New York, NY

ARTICLE INFO

Keywords:
Multimodality imaging
Quantitative imaging
Head and neck cancer
HPV+
Diffusion weighted MRI
FDG PET
Treatment response monitoring

ABSTRACT

Background and purpose: Volume regression during radiotherapy can indicate patient-specific treatment response. We aimed to identify pre-treatment multimodality imaging (MMI) metrics from positron emission tomography (PET), magnetic resonance imaging (MRI), and computed tomography (CT) that predict rapid tumor regression during radiotherapy in human papilloma virus (HPV) associated oropharyngeal carcinoma.
Materials and methods: Pre-treatment FDG PET-CT, diffusion-weighted MRI (DW-MRI), and intra-treatment (at 1, 2, and 3 weeks) MRI were acquired in 72 patients undergoing chemoradiation therapy for HPV+ oropharyngeal carcinoma. Nodal gross tumor volumes were delineated on longitudinal images to measure intra-treatment volume changes. Pre-treatment PET standardized uptake value (SUV), CT Hounsfield Unit (HU), and non-gaussian intravoxel incoherent motion DW-MRI metrics were computed and correlated with volume changes. Intercorrelations between MMI metrics were also assessed using network analysis. Validation was carried out on a separate cohort (N = 64) for FDG PET-CT.
Results: Significant correlations with volume loss were observed for baseline FDG SUV_{mean} (Spearman $\rho = 0.46$, $p < 0.001$), CT HU_{mean} ($\rho = 0.38$, $p = 0.001$), and DW-MRI diffusion coefficient, D_{mean} ($\rho = -0.39$, $p < 0.001$). Network analysis revealed 41 intercorrelations between MMI and volume loss metrics, but SUV_{mean} remained a statistically significant predictor of volume loss in multivariate linear regression ($p = 0.01$). Significant correlations were also observed for SUV_{mean} in the validation cohort in both primary ($\rho = 0.30$, $p = 0.02$) and nodal ($\rho = 0.31$, $p = 0.02$) tumors.
Conclusions: Multiple pre-treatment imaging metrics were correlated with rapid nodal gross tumor volume loss during radiotherapy. FDG-PET SUV in particular exhibited significant correlations with volume regression across the two cohorts and in multivariate analysis.

1. Introduction

Radiotherapy concurrent with chemotherapy is an important treatment modality for human papilloma virus (HPV) associated oropharyngeal carcinoma and has contributed to excellent disease control and survival rates [1,2]. Despite its efficiacy, treatment toxicity remains a major challenge in all head and neck cancers (HNC) [3,4]. Targeted dose de-escalation strategies can limit treatment-related complications without compromising locoregional control [5,6], but increasingly personalized strategies require knowledge of what factors drive variability in treatment response.

An important indicator of treatment reponse is how tumor volume evolves during therapy. Rapid volume reduction during radiotherapy is widely associated with positive outcomes in HNC [7,8]. However, just as overall response varies amongst patients, so do tumor regression rates [9] and the source of this variability is not currently well understood. Identifying characteristics that are associated with rapid intra-treatment volume regression would improve our understanding of what drives

* Corresponding author at: Department of Medical Physics, Memorial Sloan Kettering Cancer Center, 1275 Yorke Avenue, Box 84, New York, NY 10065.
E-mail address: aliottae@mskcc.org (E. Aliotta).
[1] These authors made equal contributions to this study.

https://doi.org/10.1016/j.phro.2024.100603
Received 13 March 2024; Received in revised form 19 June 2024; Accepted 20 June 2024
Available online 24 June 2024

variability in treatment response.

Multimodality imaging (MMI) may help inform this variability. For example, ^{18}F-fluorodeoxyglucose (FDG) positron emission tomography (PET), which measures local glucose metabolism, produces signals that have been linked with tumor characteristics such as proliferation [10–12], differentiation [11], and stem-ness [13] which are likely to contribute to an individual's responsiveness to treatment. Diffusion weighted Magnetic Resonance Imaging (DW-MRI), which measures the Brownian motion of water molecules, captures metrics such as the apparent diffusion coefficient (ADC) which characterize tissue cellularity [14]. Advanced DW-MRI data models such as the non-Gaussian intravoxel incoherent motion (NG-IVIM) method can additionally estimate surrogates of tissue microstructure (K, kurtosis coefficient), cellularity (D, true diffusion coefficient) and microcapillary perfusion (f, perfusion fraction and D*, pseudo-diffusion coefficient) [15]. Importantly, DW-MRI and FDG-PET provide complementary information [16] and have both been associated with clinical outcomes with high FDG uptake [17–20] and high diffusivities [21–23] being linked with poorer treatment outcomes in HNC.

We hypothesize that treatment response variability is related to characteristics of the phenotypic tumor microenvironment that can be measured using MMI. The purpose of this study was to identify the relationships between pre-treatment MMI-derived markers and longitudinal nodal gross tumor volume regression in patients with HPV+ oropharyngeal HNC.

2. Materials and methods

2.1. Patients

This study includes patients from an institutional review board approved prospective protocol (NCT03323463, Cohort-A). Eligible patients had biopsy-proven, newly diagnosed HPV-associated oropharyngeal HNC. HPV status was determined by either positive p16 expression or in situ hybridization. All patients were treated with surgery of the primary tumor followed by conventionally fractionated, intensity-modulated radiotherapy with concurrent chemotherapy [5,6]. Written informed consent was obtained from all patients included in the study.

Patients received baseline and longitudinal imaging as part of enrollment on the clinical trial. This included pre-treatment FDG PET-CT, DW-MRI, and T2-weighted MRI plus weekly MRI scans during treatment. Patients were included in the present study if all pre-treatment imaging information was available as well as weekly scans for at least 3 weeks after start of treatment. A total of 72 patients were included who were treated between November 2017 and January 2021. Seventy patients received a total radiation dose of 30 Gy to gross and subclinical disease over 3 weeks of treatment. The remaining 2 patients received a 20 fraction, 40 Gy sequential boost to gross disease (totaling 7 weeks of treatment). All patients were treated using intensity modulated radiation therapy (IMRT) with 2 Gy per fraction. Additional patient characteristics are provided in Table 1. The total imaging dataset included N = 72 pre-treatment FDG-PET scans and N = 288 MRI scans.

2.2. Imaging and segmentation

Patients underwent FDG PET-CT and MRI scans prior to treatment. FDG PET-CT imaging was performed with patients immobilized for radiotherapy treatment. 3.0 Tesla MRI scans were acquired with a protocol that included fat-suppressed T2-weighted imaging and multi-b-value DW-MRI (10 b-values, 0–2000 s/mm^2). MRI were acquired in radiological positioning (without immobilization) and were repeated weekly over the course of radiotherapy. Additional imaging details are provided in the Supplement.

Grossly involved lymph nodes were manually segmented on pre-treatment and weekly intra-treatment imaging by experienced radiation oncologists (BD, JH). Contouring was performed on both T2-weighted and DW-MRI scans (on the non-diffusion weighted b = 0 s/mm^2 series) and included the single largest lymph node for each patient.

Table 1
Patient characteristics for the primary and validation cohorts. Staging was done using the American Joint Committee on Cancer (AJCC) 7th edition tumor, node, metatstasis (TNM) system.

		Primary	Validation
	Total	72	64
Age [Years]	Median [Range]	57 [41–80]	64 [42–80]
Gender	Male	67	59
	Female	5	5
Primary Site	BOT	20	25
	Tonsil	40	28
	Unknown/Unspecified	12	11
T Stage	T0	13	1
	T1	43	15
	T2	16	24
	T3	–	11
	T4	–	12
	T4a	–	1
N Stage	N0	–	1
	N1	19	5
	N1b	–	1
	N2	8	–
	N2a	6	1
	N2b	37	31
	N2c	2	21
	N3	–	3
	N3b	–	1

2.3. Data collection and processing

DW-MRI – multi-b-value DW-MRI data were analyzed using the MRI-QAMPER (Quantitative Analysis of Multi Parametric Evaluation Routines) software platform [24] which includes monoexponential and biexponential NG-IVIM models [15] and is approved by the National Cancer Institute (NCI)/Quantitative Imaging Network (QIN) for use in clinical trials.

NG-IVIM model fits were computed to estimate true diffusion and pseudo-diffusion coefficients (D and D*), perfusion fraction (f), and Kurtosis coefficient (K) at each voxel. This method models the impact of both capillary perfusion and deviations from gaussian diffusivity (i.e. kurtosis) in highly restricted microenvironments which has been previously applied to HNC [15,25,26]. ADC maps were additionally generated using a monoexponential fit. Mean and standard deviation (SD) values of each parameter (D_{mean}, f_{mean}, D^*_{mean}, K_{mean}, and ADC_{mean}) were computed for each nodal delineation.

PET/CT – To map lesion delineations to PET-CT scans, T2-weighted MRI scans were deformably registered to the CT using a deformable b-spline algorithm with a mutual information loss function (elastix.org [27]). To avoid mapping delineations to low-resolution FDG uptake maps, PET and CT images were mapped to the T2-weighted MRI geometry, and these coregistered maps were used for all subsequent analyses.

CT Hounsfield Unit (HU) and FDG standardized uptake values (SUV) were then computed for each node. To avoid image artifacts (e.g., near dental implants), HU maps were masked to exclude regions outside the range of −100 to + 200. FDG SUV maps were generated from attenuation corrected dicom data using the "SUV Factor Calculator" 3D Slicer extension (slicer.org). CT HU_{mean}, FDG SUV_{mean}, SUV_{max}, and total lesion glycolysis (TLG) [28] were then computed across each lesion.

Weekly Volume Loss – Tumor regression was quantified using the manual delineations defined on weekly T2-weighted MRI scans. Tumor volumes (in cubic centimeters, cc) were extracted from each delineation and normalized against the pre-treatment volume to determine the fractional volume loss ($\Delta V_n = (V_{initial} - V_{week\text{-}n})/V_{initial}$ after *n* weeks of treatment, positive volume losses refering to tumor shrinkage). To correct for slight variations in scan timing and smooth week-to-week variations, ΔV were smoothed over time using a low-pass filter and linearly interpolated to exactly 1, 2, and 3 weeks after the start of radiotherapy.

Clinical Response Assessment – After the completion of treatment, clinical response was assessed monthly through follow-up FDG-PET or CT scans. At each follow-up it was determined whether or not loco-regional recurrence (LRR) was observed.

2.4. Statistical analysis

Correlations between pre-treatment imaging metrics (from DW-MRI, PET-CT) and weekly tumor regression (ΔV_1, ΔV_2, and ΔV_3) were assessed using Spearman rank-order statistics. Significant correlations were determined using a $P < 0.05$ cutoff after post-hoc Bonferroni correction.

When multiple significant correlates for ΔV were observed, predictors were fed into a multivariate linear regression model to identify independent predictors of ΔV. Only one predictor from each modality (the one with the highest correlation) was included. TLG was not used in multivariate analysis because it depends on both SUV_{mean} and total volume.

Correlations with clinical outcome were assessed using two-sample t-tests between LRR and no-LRR groups and Cox proportional hazard modelling. LRR analysis was only performed amongst patients treated with 30 Gy (70 out of 72) as all LRR were observed in this group.

These statistical analyses were performed in MATLAB (version 2022b, The Mathworks, Nattick, MA).

2.5. Network analysis

Inter-relationships between MMI and ΔV parameters were visualized using a graphical connectivity network wherein each metric defines a network node and connections between nodes represent strong inter-correlations. The presence of “communities” amongst parameters was further assessed using the “spin-glass” community detection algorithm (CDA). This approach treats each node as a “spin” and finds the best arrangement of spins, such that nodes within communities have dense coupling (i.e., strong positive or negative correlation) between them as described previously [29].

2.6. Validation cohort

An additional group of patients was included retrospectively in an IRB approved analysis (#16-1648). For this validation cohort, we selected HPV+ oropharyngeal HNC patients treated between April 2018 and June 2022 with standard-of-care conventionally-fractionated chemo-radiotherapy who received pre-treatment FDG PET-CT and weekly volumetric imaging throughout treatment (MRI or cone-beam CT, CBCT). All patients were treated using 2 Gy per fraction IMRT. Treatment was therefore equivalent to the primary cohort during the timepoints relevant to this study (the first 3 weeks of radiotherapy).

Patients were included if they underwent prospective longitudinal target-volume tracking at the time of treatment [30,31]. In this process, clinical nodal and primary gross tumor volumes (GTVn and GTVp) which were manually delineated during treatment planning were deformably propagated to each weekly MRI/CBCT (see Supplementary Methods). Pre-treatment DW-MRI was not included in this cohort due to a lack of available data with a consistent protocol.

The validation set included N = 64 patients and N = 119 GTVs (GTVn: N = 61, GTVp: N = 58). N = 42 were tracked using CBCT (66 %) and N = 22 with MRI (34 %). Correlations between baseline PET/CT parameters and weekly volume loss were computed in this cohort as in the primary analysis.

3. Results

Spearman correlations between pre-treatment imaging parameters and volume loss are shown in Fig. 1 and Table 2. Example imaging for two patients is shown in Fig. 2. Significant correlations were observed between all FDG SUV parameters (SUV_{mean}, SUV_{max}, and TLG) and ΔV_3 (SUV_{mean}/SUV_{max}/TLG: $\rho = +0.46/0.34/0.48$, $p < 0.003$). Significant correlations with ΔV_3 were also observed for D_{mean} ($\rho = -0.39$, $p < 0.001$), ADC_{mean} ($\rho = -0.37$, $p = 0.001$), and CT HU_{mean} ($\rho = +0.38$, $p = 0.001$).

When parameters from all three modalities (SUV_{mean}, D_{mean}, and HU_{mean}) were fed into a multivariate linear regression model, only SUV_{mean} remained a statistically significant predictor of ΔV_3 ($p = 0.01$, Table 2).

Significant correlations were also observed with volume losses measured at earlier time points (ΔV_1, ΔV_2) for several FDG, DW-MRI, and CT parameters (Supplementary Table S1). While correlations decreased in strength for FDG and CT parameters with ΔV_1 and ΔV_2 (eg. SUV_{mean}: $\rho = 0.34$ vs. 0.46 for ΔV_1 vs. ΔV_3), correlations were stable for DW-MRI (D_{mean}: $\rho = -0.38$ vs. -0.39 for ΔV_1 vs. ΔV_3). Fig. 1 (D–F) demonstrates the stability of these correlations over time in relative volume plots divided into three patient groups based on mean SUV_{mean}, D_{mean}, and HU_{mean}.

3.1. Network analysis

Several inter-correlations were observed between MMI parameters, which can be clearly seen in the network analysis plot shown in Fig. 3. CDA analysis revealed three distinct “communities” amongst the 12 input parameters and a connectivity network with 41 edges (each edge representing a statistically significant inter-correlation). The three communities that were identified included: 1) all volume loss measurements, ΔV_1, ΔV_2, ΔV_3; 2) All DW-MRI parameters except D^*_{mean}; and 3) All PET-CT parameters plus $V_{initial}$ and D^*_{mean}.

Full inter-correlation results are tabulated in Supplementary Table S2. Notably, SUV_{mean} was correlated with D_{mean}, (ρ = -0.49), HU_{mean} ($\rho = +0.48$), and D^*_{mean} ($\rho = -0.35$). SUV_{mean} ($\rho = 0.31$) and SUV_{max} ($\rho = 0.48$) correlated with $V_{initial}$. D_{mean} was also correlated with HU_{mean} ($\rho = -0.33$).

3.2. Treatment response assessment

LRR was observed in 7/70 patients (10.0 %) treated with 30 Gy (average follow-up time: 39 ± 10 months). Patients with LRR exhibited lower ΔV_3 (LRR: 9.5 ± 28.1 % vs. no-LRR: 38.4 ± 30.4 %, $p = 0.02$), larger $V_{week\text{-}3}$ (LRR: 23.6 ± 11.4 cc vs. no-LRR: 9.8 ± 6.8 cc, $p < 0.001$), and larger $V_{initial}$ (LRR: 28.3 ± 17.5 cc vs. no-LRR: 17.5 ± 10.9 cc, $p = 0.02$).

Cox modeling also showed significant relationships between LRR and ΔV_3 ($p = 0.03$, hazard ratio, HR = 0.98, 95 % confidence interval [0.95, 1.00]), $V_{week\text{-}3}$ ($p < 0.001$, HR = 1.20 [1.09, 1.31]), and $V_{initial}$ ($p = 0.02$, HR = 1.07 [1.01,1.12]). Kaplan-Meier curves for LRR are shown in Supplementary Fig. S2.

Significant relationships with LRR were not observed for DW-MRI or PET-CT parameters.

3.3. Validation cohort

Significant correlations were observed between FDG SUV_{mean} and ΔV_3 in the validation cohort (Table 3, Supplementary Fig. S3) for both primary (SUV_{mean}, $\rho = 0.31$) and nodal GTVs (SUV_{mean}, $\rho = 0.30$). HU_{mean} exhibited a significant correlation with ΔV_3 in the validation cohort for GTVn ($\rho = 0.33$), but not GTVp.

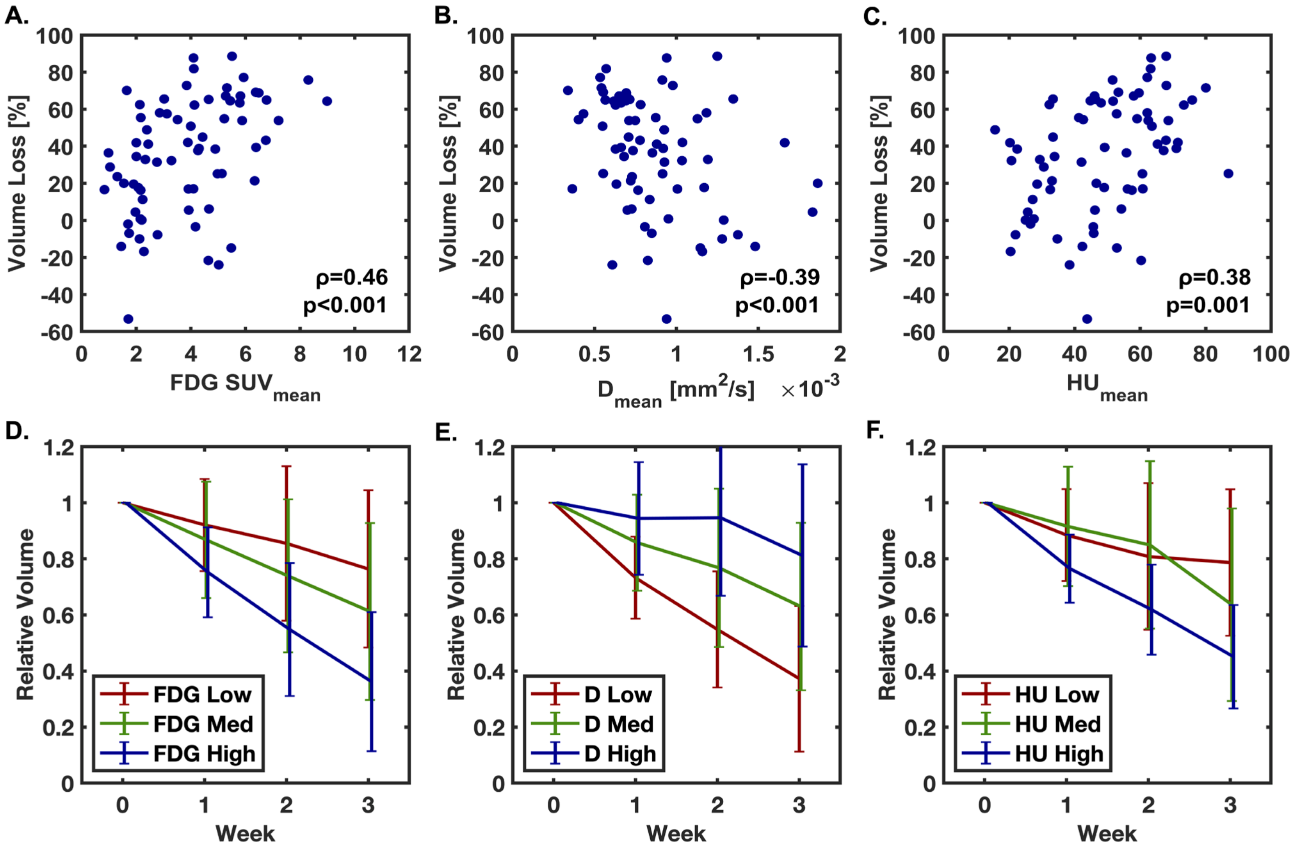

Fig. 1. Top row: plots of relative volume loss after three weeks in the primary cohort versus baseline pre-treatment imaging parameters (A–C). Bottom row: plots of relative tumor volume over time amongst all patients binned into tertiles according to baseline D) FDG SUV$_{mean}$ (cutoff values = 3.2, 5.5), E) D$_{mean}$ (cutoff values = 0.7×10^{-3}, 0.9×10^{-3}), and F) HU$_{mean}$ (cutoff values = 42.6, 60.9). Error bars represent the standard deviation of relative volumes observed within in each tertile.

Table 2
Spearman rank-order correlations between pre-treatment parameters and measured volume loss after 3 weeks of RT. Bold values were statistically significant after Bonferroni correction for multiple comparisons. NS = non-significant. Dashes indicate that a variable was not included in multivariate analysis.

		Correlation with volume loss [%]		Multivariate Regression
		ρ	p	p
FDG	SUV$_{mean}$	**0.46**	**0.00005**	**0.01**
	SUV$_{max}$	**0.34**	**0.003**	–
	TLG	**0.48**	**0.00003**	–
DW-MRI	ADC$_{mean}$	**−0.37**	**0.001**	–
	D$_{mean}$	**−0.39**	**0.0007**	NS
	f$_{mean}$	0.15	NS	–
	D*$_{mean}$	0.01	NS	–
	K$_{mean}$	−0.08	NS	–
CT	HU$_{mean}$	**0.38**	**0.001**	NS
Volume	V$_{initial}$	0.24	NS	–

4. Discussion

The main findings of this study were that (1) baseline FDG PET uptake was positively correlated with volume loss during the first three weeks of radiotherapy; and (2) other MMI metrics including CT HU and DW-MRI diffusion coefficients were both inter-correlated and correlated with volume loss.

The positive FDG-SUV correlation indicates that HPV+ oropharyngeal tumors with high baseline metabolic activity tended to regress faster during treatment than those with lower activity. In the primary cohort, this relationship was robust to FDG uptake metric (SUV$_{mean}$, SUV$_{max}$, TLG) and to the timepoint of volume measurement (weeks 1, 2, and 3). In the validation cohort, significant correlations were observed for SUV$_{mean}$ in both primary and nodal GTV, but for TLG only in GTVp. In multivariate analysis, FDG uptake was significantly correlated with nodal volume loss in both cohorts, but not for primary tumor in the validation cohort.

While we did not observe a correlation between FDG uptake and LRR, high FDG uptake has generally been associated with poor outcomes in HNC [17–20]. This would appear counter to our finding that high FDG uptake correlated with rapid regression, a characteristic associated with positive treatment outcomes in our data and elsewhere [7,8]. High FDG uptake has been associated with high density of proliferating cells across multiple cancer types [10–12] as well as a more stem-like transciptomic signature [13]. This may imply a growth-oriented and tumor-cell-dense phenotype, and may partially explain correlations that have been observed between high FDG uptake and hypoxia [32]. Tumors with high densities of cycling cells are logically more likely to regress rapidly during treatment, as has been demonstrated in radiobiological modeling studies [33,34] which may explain why high FDG uptake can relate to both poor treatment outcomes and rapid volume regression during radiotherapy. Increased proliferative activity may also bias high-FDG lesions to be larger in size at presentation (as observed in our data). Considering that absolute volumes (V$_{initial}$ and V$_{week\text{-}3}$) were associated with LRR in our data, volume bias may also play a role.

To our knowledge, the correlation between pre-treatment FDG PET uptake and volume regression has not been previously demonstrated in HNC. However, a similar finding was reported in cervical cancer by Capaldi et al. who observed high baseline FDG-uptake to be correlated with volume regression rates during chemo-radiotherapy [35]. Furthermore, a local correlation was observed in lung cancer between FDG uptake and tissue shrinkage post-treatment [36], which indicates that this relationship may not be limited to HPV+ oropharyngeal cancer.

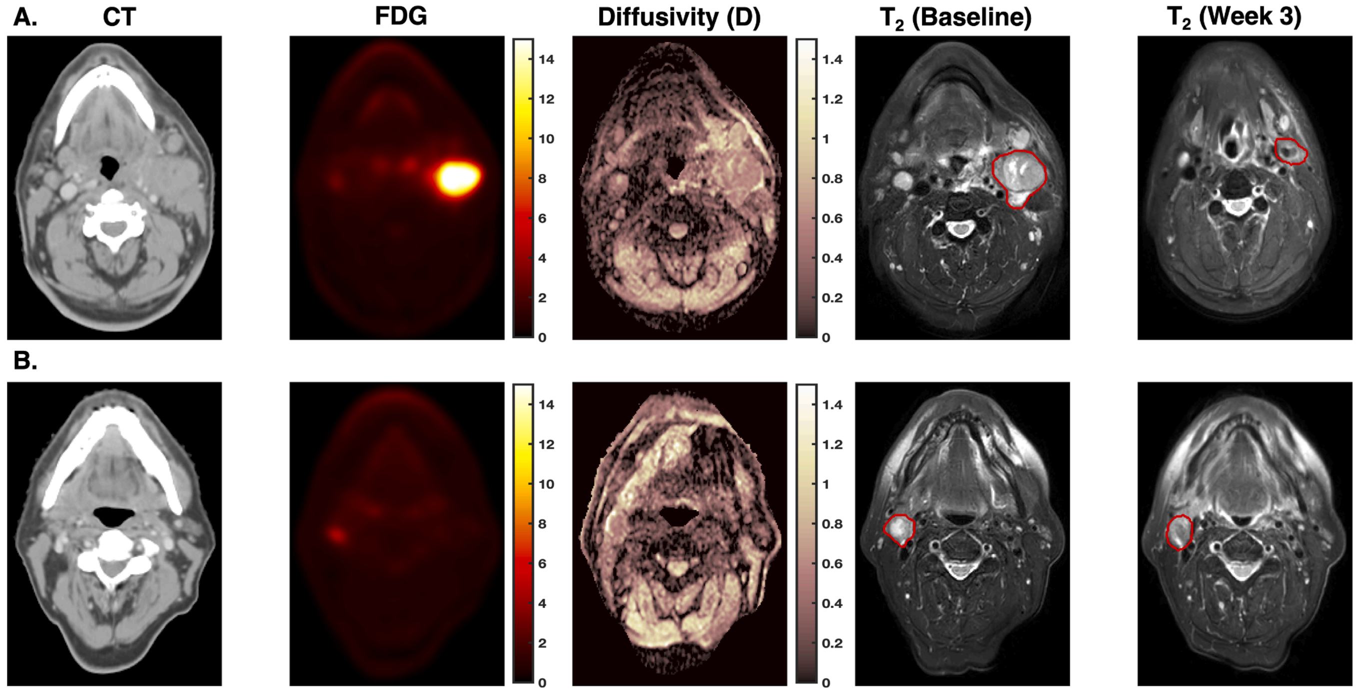

Fig. 2. Example pre-treatment and week-3 imaging for two patients in this study. The patient in panel A (male, age 56 years) showed high baseline FDG uptake (SUV_{mean} = 8.3) and exhibited >75 % volume loss upon week-3 imaging. In contrast, the patient in panel B (Male, age 67 years) showed pre-treatment SUV_{mean} = 2.15 and only 0.8 % volume loss at week-3 of treatment.

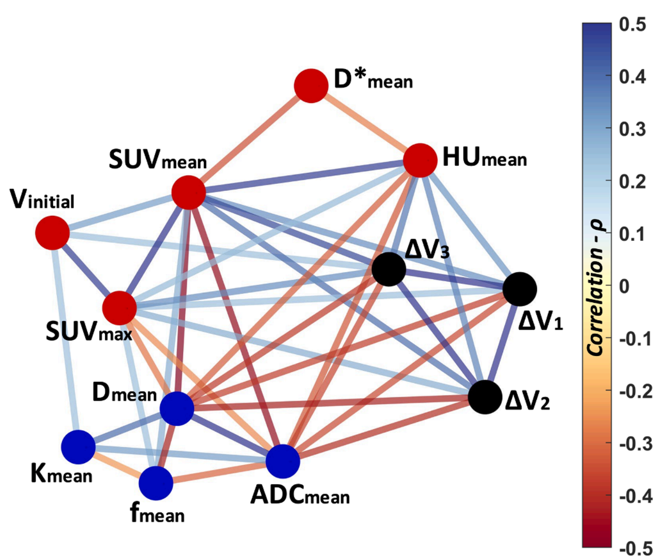

Fig. 3. Intercorrelation network between MMI parameters generated from a community detection algorithm (CDA) based on the "spin-glass" model. Network nodes represent individual MMI parameters and connections between them represent correlations with $P < 0.05$. Line color indicates the spearman rank-order correlation coefficient (ρ) of that connection (blue lines indicate positive correlations and red lines indicate negative correlations). Node color indicates the three parameter "communities" determined by the CDA. Note that perfusion fraction (f) and pseudo-diffusion coefficient (D*) metrics are currently experimental and not yet validated clinically. (For interpretation of the references to color in this figure legend, the reader is referred to the web version of this article.)

We also observed correlations between volume loss and both baseline diffusivities (negative correlation) and CT HU values (positive correlation). Both low diffusivities and high HU values are indicative of dense tissue (though in contrast-enhanced CT, HU values are also affected by extracellular contrast), implying that dense tumors are more likely to exhibit rapid volume loss. This is consistent with previous studies which associated low pre-treatment diffusivities with superior outcomes in HNC [21–23]. D_{mean} and HU_{mean} were also both significantly correlated with SUV_{mean} and neither D_{mean} nor HU_{mean} were significant multivariate predictors of volume loss, which may indicate that high cell density is a consequence of the increased proliferation in high-FDG tumors.

One potential application for these findings is in the growing field of "digital-twin" research wherein patient-specific treatment response is predicted and monitored with radiobiological models. Tumor volume regression serves as an important input and/or feedback mechanism in several published methods [33,37–39]. Knowledge of the relationships between intra-treatment regression and imaging characteristics may inform future strategies to initialize and update personalized models with MMI data.

The CDA network analysis (Fig. 3) was largely consistent with analysis by Paudyal et al. who also reported significant correlations between FDG uptake and both D/ADC (negative correlations) and tumor volume (positive correlation) [29]. In the present study, three communities were identified amongst the MMI parameters and they were largely grouped within modalities. This indicates that intra-modality correlations were generally stronger than inter-modality (aside from D*, which was grouped with PET-CT parameters but is an exploratory, unvalidated parameter with known variability [40]). However, it is clear from the densely connected network graph that many connections exist between communities.

One important variable not addressed in this study is the presence of cystic lymph nodes, which are most commonly observed in HPV+ cancers [41] and tend to exhibit both high diffusivity and low FDG uptake due to the high water content and lack of cancer cells in cystic regions. Because cystic tissue would also not be expected to regress quickly during radiotherapy, this may have contributed to the observed correlations and is a limitation of our study. Furthermore, because grossly involved lymph nodes are not composed entirely of tumor cells, a decrease in nodal volume is not directly indicative of a decrease in tumor

Table 3
Spearman rank-order correlations between each pre-treatment parameters and measured volume loss after 3 weeks of RT in the validation cohort. Bold values were statistically significant ($P < 0.05$). NS = non-significant. Dashes indicate that a variable was not included in multivariate analysis.

		Validation – GTVn			Validation – GTVp		
		Correlation with volume loss [%]		Multivariate Regression	Correlation with volume loss [%]		Multivariate Regression
		ρ	p	p	ρ	p	p
FDG	SUV_{mean}	**0.31**	**0.02**	**0.01**	**0.30**	**0.02**	NS
	SUV_{max}	0.22	NS	–	0.26	NS	–
	TLG	0.21	NS	–	**0.32**	**0.01**	–
CT	HU_{mean}	**0.33**	**0.009**	**0.05**	0.08	NS	–
Volume	$V_{initial}$	0.12	NS	–	**0.28**	**0.03**	NS

burden. Although the validation cohort did show a correlation between FDG uptake and volume loss in primary tumor, future analysis will aim to exclude cystic components from lesion delineations and limit analysis to regions of active tumor.

This study had some additional limitations. Namely, it was a retrospective, single-center study which always carries some risk of bias. However, the primary cohort was a consecutive group of patients who had MMI acquired during a prospective trial (NCT03323463). We also hope to have mitigated this risk by replicating our main findings in a separate cohort. However, the validation cohort did differ from the primary group in the use of automatic propagation of clinical GTVs to compute volume trends and the inclusion of primary tumor, which may have affected the results. Another limitation was that the only marker of longitudinal treatment response that we evaluated was tumor volume. Changes in DW-MRI and/or PET-CT parameters may provide additional insight into how tumor composition changes throughout treatment. Furthermore, the low LRR rate (10 %) led to a small number of events observed. Additional parameters may have exhibited significant relationships with outcome in a larger sample. Finally, volume changes were only assessed until week-3 of radiotherapy, although we expect treatment-induced changes to persist in subsequent weeks. However, because many of the patients only received three weeks of treatment, this was the latest time point in which all patients in both cohorts had received an equivalent dose.

In conclusion, MMI parameters were associated with rapid volume regression during radiotherapy for HPV+ oropharyngeal cancer. Pretreatment FDG uptake had the strongest correlation with volume loss in both uni- and multivariate analysis.

Funding statement

This research was funded in part through NIH R01 CA238392-02A1, NIH R01 CA157770-01A1 and the NIH/NCI Cancer Center Support Grant P30 CA008748.

CRediT authorship contribution statement

Eric Aliotta: Conceptualization, Methodology, Software, Writing – original draft. **Ramesh Paudyal:** Data curation, Validation, Resources, Writing – review & editing, Formal analysis. **Bill Diplas:** Data curation, Writing – review & editing. **James Han:** Data curation, Writing – review & editing. **Yu-Chi Hu:** Software, Methodology. **Jung Hun Oh:** Software, Methodology, Writing – review & editing. **Vaios Hatzoglou:** Data curation, Writing – review & editing. **Naomi Jensen:** Data curation, Formal analysis. **Peng Zhang:** Data curation, Software. **Michalis Aristophanous:** Data curation, Validation, Resources, Writing – review & editing. **Nadeem Riaz:** Conceptualization, Data curation, Validation, Resources, Writing – review & editing. **Joseph O. Deasy:** Conceptualization, Resources, Writing – review & editing. **Nancy Y. Lee:** Conceptualization, Resources, Writing – review & editing, Data curation. **Amita Shukla-Dave:** Conceptualization, Resources, Validation, Writing – review & editing, Data curation.

Declaration of competing interest

The authors declare the following financial interests/personal relationships which may be considered as potential competing interests: Nancy Lee receives consulting fees from Shanghai Joanne Medical Ltd, Yingming Consulting, and Varian, has support from a Varian travel grant, and is on the advisory board for Merck, Merck Serono, Merck EMD, Nanobiotix, and Regeneron. Nadeem Riaz receives research support from Invitae, Pfizer, and Repare Therapuetics.

Appendix A. Supplementary data

Supplementary data to this article can be found online at https://doi.org/10.1016/j.phro.2024.100603.

References

[1] Ang KK, Harris J, Wheeler R, Weber R, Rosenthal DI, Nguyen-Tân PF, et al. Human papillomavirus and survival of patients with oropharyngeal cancer. N Engl J Med 2010 Jul 1;363(1):24–35.
[2] Pfister DG, Spencer S, Adelstein D, Adkins D, Anzai Y, Brizel DM, et al. Head and neck cancers, version 2.2020. J Natl Compr Canc Netw 2020 Jul 1;18(7):873–98.
[3] van der Laan HP, Van den Bosch L, Schuit E, Steenbakkers RJHM, van der Schaaf A, Langendijk JA. Impact of radiation-induced toxicities on quality of life of patients treated for head and neck cancer. Radiother Oncol 2021 Jul;1(160):47–53.
[4] Osazuwa-Peters N, Simpson MC, Zhao L, Boakye EA, Olomukoro SI, Deshields T, et al. Suicide risk among cancer survivors: Head and neck versus other cancers. Cancer 2018 Oct 15;124(20):4072–9.
[5] Riaz N, Sherman E, Pei X, Schöder H, Grkovski M, Paudyal R, et al. Precision radiotherapy: reduction in radiation for oropharyngeal cancer in the 30 ROC trial. J Natl Cancer Inst 2020 Jun 1;00(6):742–51.
[6] Lee NY, Sherman EJ, Schöder H, Wray R, Boyle JO, Singh B, et al. Hypoxia directed Treatment of human papillomavirus related oropharyngeal carcinoma. J Clin Oncol 2023.
[7] Jaulerry C, Dubray B, Brunin F, Rodriguez J, Point D, Blaszka B, et al. Prognostic value of tumor regression during radiotherapy for head and neck cancer: a prospective study. Int J Radiat Oncol Biol Phys 1995 Sep 30;33(2):271–9.
[8] Liang SB, Zhang N, Chen DM, Yang XL, Chen BH, Zhao H, et al. Prognostic value of gross tumor regression and plasma Epstein Barr Virus DNA levels at the end of intensity-modulated radiation therapy in patients with nasopharyngeal carcinoma. Radiother Oncol 2019 Mar;1(132):223–9.
[9] Barker JL, Garden AS, Ang KK, O'Daniel JC, Wang H, Court LE, et al. Quantification of volumetric and geometric changes occurring during fractionated radiotherapy for head-and-neck cancer using an integrated CT/linear accelerator system. Int J Radiat Oncol Biol Phys 2004 Jul 15;59(4):960–70.
[10] Minn H, Joensuu H, Ahonen A, Klemi P. Florodeoxyglucose imaging: A method to assess the proliferative activity of human cancer in vivo. Comparison with DNA flow cytometry in head and neck tumors. Cancer 1988;61(9):1776–81.
[11] Vesselle H, Salskov A, Turcotte E, Wiens L, Schmidt R, Jordan CD, et al. Relationship between non-small cell lung cancer FDG uptake at PET, Tumor HISTOLOGY, and Ki-67 proliferation index. J Thorac Oncol 2008 Sep 1;3(9):971–8.
[12] Haberkorn U, Strauss LG, Reisser C, Haag D, Dimitrakopoulou A, Ziegler S, et al. Glucose uptake, perfusion, and cell proliferation in head and neck tumors: Relation of positron emission tomography to flow cytometry. J Nucl Med 1991;32(8):1548–55.
[13] Riester M, Xu Q, Moreira A, Zheng J, Michor F, Downey RJ. The Warburg effect: Persistence of stem-cell metabolism in cancers as a failure of differentiation. Ann Oncol 2018 Jan 1;29(1):264–70.
[14] Surov A, Meyer HJ, Wienke A. Correlation between apparent diffusion coefficient (ADC) and cellularity is different in several tumors: a meta-analysis. Oncotarget 2017;8(35):59492.
[15] Lu Y, Jansen JFA, Mazaheri Y, Stambuk HE, Koutcher JA, Shukla-Dave A. Extension of the intravoxel incoherent motion model to non-gaussian diffusion in head and neck cancer. J Magn Reson Imaging 2012 Nov;36(5):1088–96.

[16] Houweling AC, Wolf AL, Vogel WV, Hamming-Vrieze O, Van Vliet-Vroegindeweij C, Van De Kamer JB, et al. FDG-PET and diffusion-weighted MRI in head-and-neck cancer patients: Implications for dose painting. Radiother Oncol 2013 Feb 1;106(2):250–4.

[17] Paidpally V, Chirindel A, Lam S, Agrawal N, Quon H, Subramaniam RM. FDG-PET/CT imaging biomarkers in head and neck squamous cell carcinoma. Imaging Med 2012 Dec;4(6):633.

[18] Zhang B, Li X, Lu X. Standardized uptake value is of prognostic value for outcome in head and neck squamous cell carcinoma [Internet]. Vol. 130, Acta Oto-Laryngologica. Taylor & Francis; 2010. p. 756–62. Available from: https://www.tandfonline.com/doi/abs/10.3109/00016480903402981.

[19] Cho H, Kim S, Jo K, Jeong YH, Kang WJ. Tumor glucose metabolism and its heterogeneity on F-18 FDG PET/CT provide better prognostication in nonmetastatic human papillomavirus-related oropharyngeal squamous cell carcinoma. Available from: Cancers [Internet] 2021 Nov 1;13(21). https://www.ncbi.nlm.nih.gov/pmc/articles/PMC8583647/.

[20] Jeong J, Setton JS, Lee NY, Oh JH, Deasy JO. Estimate of the impact of FDG-avidity on the dose required for head and neck radiotherapy local control. Radiother Oncol 2014;111(3):340–7.

[21] King AD, Thoeny HC. Functional MRI for the prediction of treatment response in head and neck squamous cell carcinoma: potential and limitations. Available from: Cancer Imaging [Internet] 2016 Aug 19;16(1). https://pubmed.ncbi.nlm.nih.gov/27542718/.

[22] Martens RM, Noij DP, Koopman T, Zwezerijnen B, Heymans M, de Jong MC, et al. Predictive value of quantitative diffusion-weighted imaging and 18-F-FDG-PET in head and neck squamous cell carcinoma treated by (chemo)radiotherapy. Eur J Radiol 2019 Apr;1(113):39–50.

[23] Martens RM, Koopman T, Lavini C, Ali M, Peeters CFW, Noij DP, et al. Multiparametric functional MRI and 18F-FDG-PET for survival prediction in patients with head and neck squamous cell carcinoma treated with (chemo) radiation. Eur Radiol 2021 Feb 1;31(2):616–28.

[24] LoCastro E, Paudyal R, Konar AS, LaViolette PS, Akin O, Hatzoglou V, et al. A quantitative multiparametric MRI analysis platform for estimation of robust imaging biomarkers in clinical oncology. Tomography 2023 Nov 3;9(6):2052–66.

[25] Paudyal R, Chen L, Oh JH, Zakeri K, Hatzoglou V, Tsai CJ, et al. Nongaussian intravoxel incoherent motion diffusion weighted and fast exchange regime dynamic contrast-enhanced-MRI of nasopharyngeal carcinoma: preliminary study for predicting locoregional failure. Available from: Cancers [Internet] 2021 Mar 6; 13(5). https://doi.org/10.3390/cancers13051128.

[26] Paudyal R, Riaz N, Hatzoglou V, Lee N, Shukla-Dave A. Non-gaussian IVIM-DWI for HPV-related oropharyngeal cancer patients who received marked dose de-escalation in chemo-radiotherapy: Intra-treatment imaging response evaluation. Proc Intl Soc Mag Reson Med 2019:2358.

[27] Klein S, Staring M, Murphy K, Viergever MA, Pluim JP. elastix: a toolbox for intensity-based medical image registration. IEEE Trans Med Imaging 2010;29(1): 196–205.

[28] Larson SM, Erdi Y, Akhurst T, Mazumdar M, Macapinlac HA, Finn RD, et al. Tumor treatment response based on visual and quantitative changes in global tumor glycolysis using PET-FDG imaging: the visual response score and the change in total lesion glycolysis. Clin Positron Imaging 1999 May 1;2(3):159–71.

[29] Paudyal R, Grkovski M, Oh JH, Schöder H, Nunez DA, Hatzoglou V, et al. Application of community detection algorithm to investigate the correlation between imaging biomarkers of tumor metabolism, hypoxia, cellularity, and perfusion for precision radiotherapy in head and neck squamous cell carcinomas. Available from: Cancers [Internet] 2021 Aug 1;13(15). https://pubmed.ncbi.nlm.nih.gov/34359810/.

[30] Aliotta E, Hu YC, Zhang P, Lichtenwalner P, Caringi A, Allgood N, et al. Automated tracking of morphologic changes in weekly magnetic resonance imaging during head and neck radiotherapy. J Appl Clin Med Phys 2023 May;5:e13959.

[31] Aristophanous M, Aliotta E, Lichtenwalner P, Abraham S, Nehmeh M, Caringi A, et al. Clinical experience with an offline adaptive radiation therapy head and neck program: dosimetric benefits and opportunities for patient selection. Available from: Radiat Oncol Biol Phys [Internet] Feb 17 2024. https://doi.org/10.1016/j.ijrobp.2024.02.016.

[32] Crispin-Ortuzar M, Apte A, Grkovski M, Oh JH, Lee NY, Schöder H, et al. Predicting hypoxia status using a combination of contrast-enhanced computed tomography and [18F]-Fluorodeoxyglucose positron emission tomography radiomics features. Radiother Oncol 2018 Apr;127(1):36–42.

[33] Prokopiou S, Moros EG, Poleszczuk J, Caudell J, Torres-Roca JF, Latifi K, et al. A proliferation saturation index to predict radiation response and personalize radiotherapy fractionation. Radiat Oncol 2015 Jul 31;10(1):1–8.

[34] Jeong J, Shoghi KI, Deasy JO. Modelling the interplay between hypoxia and proliferation in radiotherapy tumour response. Phys Med Biol 2013 Jul 21;58(14): 4897–919.

[35] Capaldi DPI, Hristov DH, Kidd EA. Parametric response mapping of coregistered positron emission tomography and dynamic contrast enhanced computed tomography to identify radioresistant subvolumes in locally advanced cervical cancer. Int J Radiat Oncol Biol Phys 2020;107(4):756–65.

[36] Zhang P, Alam S, Thor M, Rimner A, Deasy J, Lu W. Correlation between metabolic uptake in planning PET and end-of-RT tumor change in lung cancer. Med Phys 2022 Jun;49(6).

[37] Zahid MU, Mohsin N, Mohamed ASR, Caudell JJ, Harrison LB, Fuller CD, et al. Forecasting individual patient response to radiation therapy in head and neck cancer with a dynamic carrying capacity model. Int J Radiat Oncol Biol Phys 2021 Nov 1;111(3):693–704.

[38] Browning AP, Lewin TD, Baker RE, Maini PK, Moros EG, Chaudell J, et al. Predicting radiotherapy patient outcomes with real-time clinical data using mathematical modelling. Bull Math Biol 2024 Jan 18;86(2):19.

[39] Sunassee ED, Tan D, Ji N, Brady R, Moros EG, Caudell JJ, et al. Proliferation saturation index in an adaptive Bayesian approach to predict patient-specific radiotherapy responses. Int J Radiat Biol 2019 Oct 3;95(10):1421–6.

[40] Noij DP, Martens RM, Marcus JT, de Bree R, Leemans CR, Castelijns JA, et al. Intravoxel incoherent motion magnetic resonance imaging in head and neck cancer: a systematic review of the diagnostic and prognostic value. Oral Oncol 2017 May;68:81–91.

[41] Goldenberg D, Begum S, Westra WH, Khan Z, Sciubba J, Pal SI, et al. Cystic lymph node metastasis in patients with head and neck cancer: An HPV-associated phenomenon. Head Neck 2008 Jul;30(7):898–903.